RESEARCH ARTICLE

Electrodeposition of lead dioxide on Fe electrode: application to the degradation of Indigo Carmine dye

Sabrina Tabti[1] · Abdelkader Benchettara[1] · Fatiha Smaili[1] · Abdelhakim Benchettara[1] · Salah Eddine Berrabah[1]

Abstract

The modification of an iron electrode was carried out according to the following two steps. In a first step, a cathodic reduction is performed to form a film of metallic lead on a bare iron electrode, in 5 mol m^{-3} + 50 mol m^{-3} KNO$_3$ solution, at −0.8 V/SCE during 300 s. In a second step, the film of metallic lead is converted to PbO$_2$ in 100 mol m^{-3} NaOH solution, at + 0.7 V/SCE during 150 s. EDX, X-ray diffraction and scanning electron microscopy analysis, confirm that Pb metal and α-PbO$_2$ are successfully deposited. The electrocatalytic activity of the resulting oxide is assessed for the indigo-carmine (IC) dye degradation reaction, using potentiostatic method. The IC dye was successfully oxidized by hydroxyl radical electrogenerated from oxidation of water on the Fe/Pb/α-PbO$_2$ electrode. These results suggest that Fe/Pb/α-PbO$_2$ electrode is a promising candidate for electrocatalytic degradation of IC wastewater.

Graphical abstract
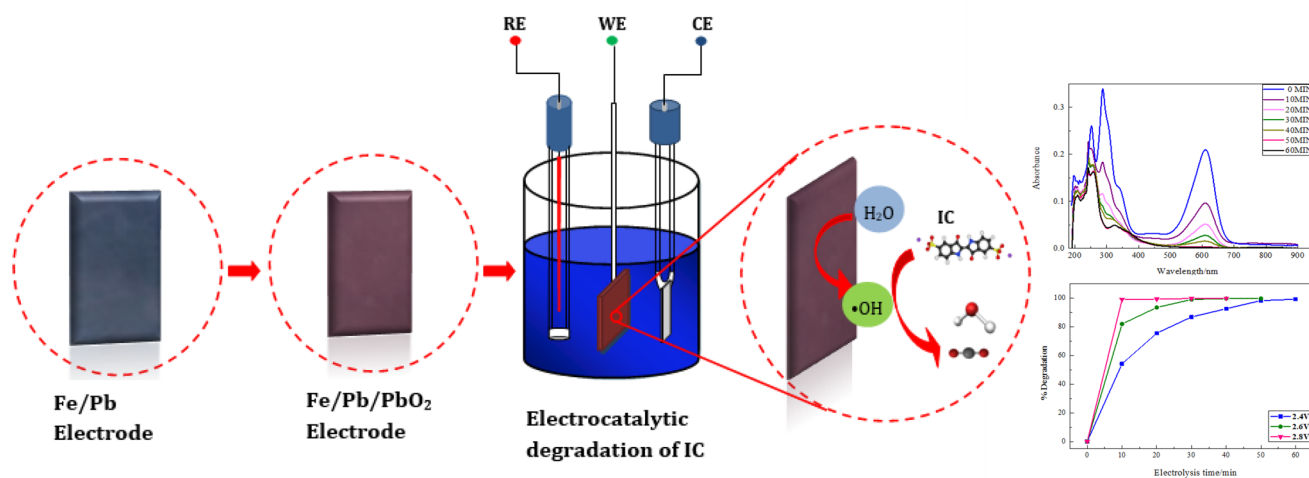
✉ Sabrina Tabti
  tabti.dz@gmail.com

1   Laboratory of Electrochemistry-Corrosion, Metallurgy
    and Inorganic Chemistry, Faculty of Chemistry, (USTHB)
    BP 32, El Alia Bab Ezzouar, 16111 Algiers, Algeria

1 Introduction

With the rapid development of the economy and progress of industrial technology, the pollution of organic wastewater has become increasingly serious. Among all the types of pollution, dye wastewater produced by the printing industry, leather, textile, plastics and paper is extremely harmful to the environment [1, 2]. Various

treatment processes have been applied to remove dye from wastewaters, such as biological degradation[3], coagulation–flocculation [4], Fenton's oxidation [5], membrane separation [6] and photocatalysis [7]. However, these processes are quite expensive and have operational problems [8]. Among all these methods, electrochemical catalytic oxidation technology has elicited considerable attention because of its significant advantages, such as environmental compatibility, a lack of chemical reagents, ease of operation, thorough degradation of pollutants, and lack of secondary pollution [9]. In the long term, lead dioxide can contribute substantially to a fundamental understanding of the relationship between the coating structure and catalytic activity, important to all fields of catalysis [10]. The methods for the preparation of electrodes include electrodeposition, pressing-sintering, microwave plasma chemical vapour deposition and thermal decomposition [11], among these methods, electrodeposition possesses favorable characteristics, such as simplicity, easy control and environmental compatibility [12].

Lead dioxide coatings have a low cost compared to those based on precious metals, a high electrical conductivity (comparable to metals), a high oxygen overpotential and a good stability in controlled conditions leading to possible applications in new processes [10]. The electrodeposition of PbO_2 has been studied on many substrates such as glassy-carbon [13], gold [14], platinum [15], graphite [16, 17], titanium [18], lead [19], using different electrolytes as nitric acid [20], perchloric acid [21], methanesulfonic acid [22], and different additives to prepare composites [23].

The industrial-scale mineralization requires the use of a high surface area electrode. For this reason, we selected an iron Fe substrate, because of its inexpensive cost compared to gold or platinum substrates, as well as for its availability on the Algerian market, and everywhere else. The use of this new electrode, also allows enriching the databases of the literature, contrary to those in graphite, glassy carbon… etc. Which have been widely studied.

In order to study the anodic oxidation of dyes on an electrode coating, this work focused in a first step to the preparation of a lead dioxide film (PbO_2) on iron substrate by the electrochemical method, in a second step to study the electrochemical oxidation process of the degradation of indigo carmine (IC) in an aqueous solution Indigo Carmine (IC) is obtained from indigo dye through a chemical reaction with sulfuric acid. IC is considered a highly toxic indigoid class of dye and constitutes one of the most important groups of pollutants found in wastewaters from textile industries. It was used in many industries, such as plastics, textile, and papers industries, and it is used as indicator in analytical chemistry, as food coloring and as microscopic stain in biology. Some papers have shown that IC can react with H_2O_2 producing serious pollution in water [24].

2 Experimental

2.1 Materials and reagents

All chemicals substances employed in this work were of analytical grade. The solutions used for all experiments were prepared using distilled water pH = 6.65. In this study, we have used the potassium nitrate (KNO_3, Fluka, 99%) as supporting electrolyte. Lead nitrate ($Pb(NO_3)_2$, Riedel_de Haën, 99.5%) is used for modifying an iron substrate (purity: 99.3%) with a lead film. Sodium hydroxide (NaOH, Biochem, 98%) is used for converting anodically lead to lead dioxide electrode. To improve the conductivity of the solution and to achieve better degradation, the dye solution was prepared by 10^{-2} mol m^{-3} indigo carmine (Reagenzien Merck) in 50 mol m^{-3} KNO_3, the solution pH was adjusted with HNO_3, KOH solutions. A conventional three-electrode cell was used to do the electrochemical experiments, and the electrochemical measurements were conducted at 25 °C in glass cell, using a potentiostat model Solartron SI 1287, controlled by CorrWave software. For the electrode modifications, a saturated calomel electrode (SCE) filled with KCl was used as the reference (XR 110, Radiometer), a platinum plate as the counter electrode and an iron electrode with a surface area of 1.13 cm^2 as the working electrode, however, larger surfaces are required for the electrodegradation, therefore, the counter and the working electrodes were replaced by, a stainless steel plate and 30 cm^2 iron electrode, respectively. The iron electrode was polished (Mecapol Presi-type 2B), under running water with abrasive paper 800/1200, before each test, washed with acetone and was rinsed with distilled water to remove any residues from the polishing process.

Cyclic voltammetry tests were performed in an aqueous solution of 50 mol m^{-3} KNO_3 in absence and presence of 5 mol m^{-3} Pb ($NO_3)_2$, the potential sweep was carried out in the cathodic direction at a scan rate of 5 mV s^{-1}. Furthermore, in order to determine the different interfacial electron transfer reactions that can take place at the Pb /100 mol m^{-3} NaOH interface, a cyclic voltammogram was carried out in the anodic direction at a potential range from −1.3 V to 0.8 V/SCE, with a potential sweep of 10 mV s^{-1}.

The EIS measurements were performed for unmodified and modified iron electrode, in 50 mol m^{-3} KNO_3 at free potential and in a frequency range between 10^5 and 10^{-2} Hz with an amplitude of 10 mV. The impedance data were analyzed and fitted to electrical equivalent circuits with Zview software.

Accelerated lifetime test was conducted in 500 mol m^{-3} KNO_3 with current density of 1000 mA cm^{-2} at 25 °C. to evaluate the chemical stability of the prepared electrode.

The LSV of the Fe/Pb/α-PbO$_2$ modified electrode was performed in 50 mol m^{-3} KNO$_3$ in the range from 0.4 to 3 V/SCE at a scanning speed of 25 mV s^{-1}.

2.2 Analysis

The surface morphologies of the films were observed by a FEI QUANTA 650 scanning electron microscopy with EDX (BRUKER), to analyze the composition of the films, the structure of the films were analyzed by X-ray diffraction (XRD) PANALYTICAL EMPYREAN.

The electrocatalytic degradation of IC was monitored by UV–Vis spectrophotometer Jascov 650 from 190 to 900 nm. The maximum wavelength absorbance (λmax) of IC was located at 610 nm from the spectra. Thus, the residual concentration of the dye in the reaction mixture at different reaction times was calculated by measuring the absorption intensity at λmax = 610 nm from a calibration curve.

The efficiency of color removal was expressed from the following relation 1 [25]:

$$\text{Efficiency (\%)} = \left(1 - \frac{C_t}{C_0}\right) \tag{1}$$

where C$_0$ and C$_t$ are the concentrations of IC at reaction times.

UV–VIS spectrophotometer DR 6000 was used to measure the solution TOC.

3 Results and discussion

3.1 Elaboration of Pb film

3.1.1 Cyclic voltammetry

In order to delimit the potential range of lead deposition on iron, we carried out a preliminary study by cyclic voltammetry (Fig. 1). The cyclic voltammogram curve of 50 mol m^{-3} KNO$_3$ shows no oxidation or reduction peaks on the iron in the explored potential range; the stability domain of the supporting electrolyte used gives off a sufficient electrochemical window (−0.2 to −1 V/SCE) to study the electrochemical behavior of lead on iron. But after addition of 5 mol m^{-3} Pb(NO$_3$)$_2$ to 50 mol m^{-3} KNO$_3$ (pH = 5.4), a cathodic peak appears at −0.55 V/SCE corresponding to the reduction of Pb (II) ions to metallic lead on the iron surface according to Eq. (2).
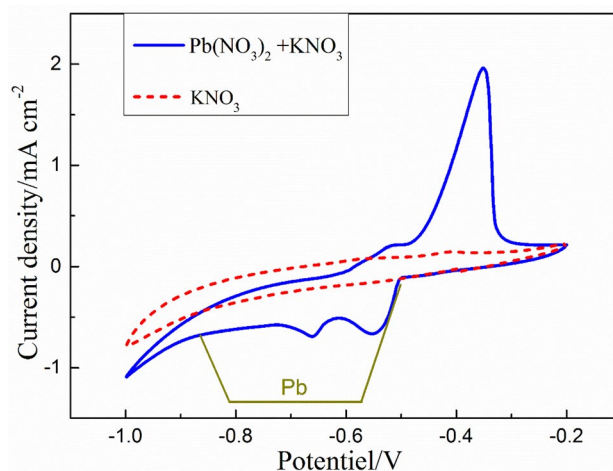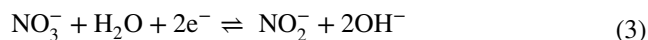
$$\text{Pb}^{2+} + 2\,\text{e}^- \rightleftharpoons \text{Pb}_\text{s} \tag{2}$$

Fig. 1 Cyclic voltammetry of Fe in 5 mol m^{-3} Pb (NO$_3$)$_2$ + 50 mol m^{-3} KNO$_3$ solution, T = 25 °C, at a scan rate of 5 mV s^{-1}

Another peak appears at −0.66 V/SCE attributed to the reduction of nitrate ions to nitrite (NO$_3^-$/NO$_2^-$) according to Eq. (3), followed by the reduction of water.

$$\text{NO}_3^- + \text{H}_2\text{O} + 2\text{e}^- \rightleftharpoons \text{NO}_2^- + 2\text{OH}^- \tag{3}$$

The reduction reaction of nitrate ions to nitrite ions can be interpreted by the lead metal film has catalytic effects on the reduction of nitrate ions.

3.1.2 Chronoamperometry

By exploiting the results of the voltammogram in Fig. 1, we were able to choose the potential to apply to deposit lead film. The lead was deposited on iron by chronoamperometry at a potential E = −0.8 V/SCE for 300 s.

The Fig. 2 shows that the current density in absolute value decreases rapidly from the first moments of deposition and continues to decrease slowly then it stabilizes. The decrease of the current is due to the progressive covering of the iron surface by the lead.

After depositing the lead metal and removing the coated iron electrode from the solution, a change in the deposit color is noticed after a moment of exposure to air. In this step two samples are prepared, the first one is rinsed with ethanol and dried quickly after removing it from the solution, the second one is dried slowly in air at room temperature.
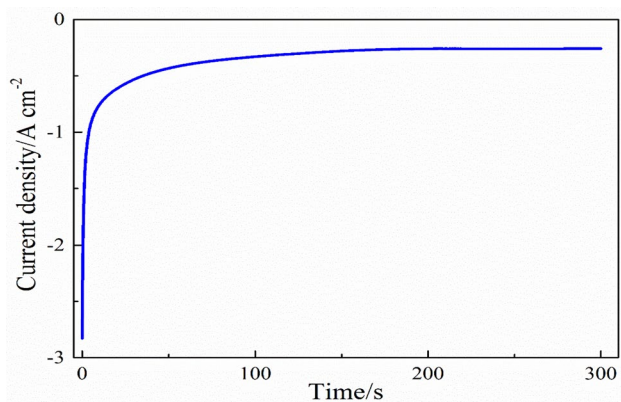
Fig. 2 Chronoamperometry of iron electrode in 5 mol m^{-3} Pb(NO$_3$)$_2$ + 50 mol m^{-3} KNO$_3$ solution, E = −0.8 V, at 25 °C

3.2 Conversion of Pb on PbO$_2$

3.2.1 Cyclic voltammetry

A cyclic voltammetry test was to determine the different interfacial electron transfer reactions that can take place at the Pb / 100 mol m^{-3} NaOH interface.

The voltammogram in Fig. 3 shows three anodic peaks in the forward sweep: the first peak is located at −0.58 V (A$_1$), second one at −0.15 V (A$_2$) and a third one at +0.59 V (A$_3$). But in the backward sweep, a large cathodic peak appears at −0.05 V (C$_1$), an another peak at −0.9 V (C$_2$) and a last cathodic peak is observed at −1.15 (C$_3$).

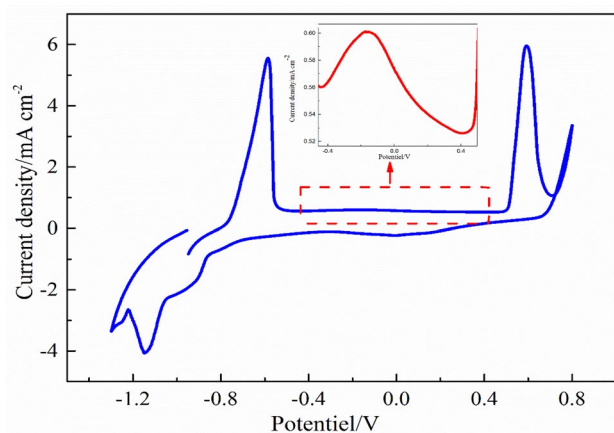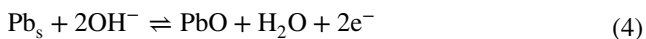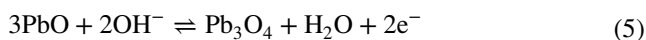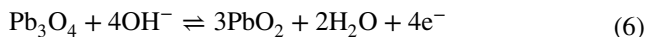The peak (A$_1$) corresponds to the anodic oxidation of Pb to PbO according to the Eq. (4).

$$Pb_s + 2OH^- \rightleftharpoons PbO + H_2O + 2e^- \tag{4}$$

The peak (A$_2$) corresponds to the anodic oxidation of PbO to Pb$_3$O$_4$ according to the Eq. (5).

$$3PbO + 2OH^- \rightleftharpoons Pb_3O_4 + H_2O + 2e^- \tag{5}$$

The peak (A$_3$) corresponds to the anodic oxidation of Pb$_3$O$_4$ to PbO$_2$ according to the Eq. (6).

$$Pb_3O_4 + 4OH^- \rightleftharpoons 3PbO_2 + 2H_2O + 4e^- \tag{6}$$

The (C$_1$) peak represents the reduction of PbO$_2$ to Pb$_3$O$_4$, the (C$_2$) to the reduction of Pb$_3$O$_4$ to PbO, and (C$_3$) to the reduction of PbO to Pb.

The analysis of this voltammogram allowed us to choose the adequate potential for the oxidation of metallic lead to lead dioxide.

3.2.2 Chronoamperometry

The chronoamerogram in Fig. 4 shows that the current decreases rapidly in the first few seconds and continues to decrease moderately then stabilizes at a constant value. The decrease of the current is due to the progressive coverage of the lead surface by the lead dioxide and the constant value reflects the fact that the diffusion of ions in the solution becomes the limiting step for the growth of the deposited film.

3.3 Characterization of films

EDX spectra show only the presence of metallic lead and iron in quick-drying with air electrode, as well as the presence of lead, oxygen and iron in the slowly air-dried sample, indicating that the metallic lead has been oxidized in air to lead oxides (Fig. 5a). The SEM photographs of these films also reveal a clear difference (Fig. 5b) in the morphology, and to identify the oxides formed in the air a DRX analysis
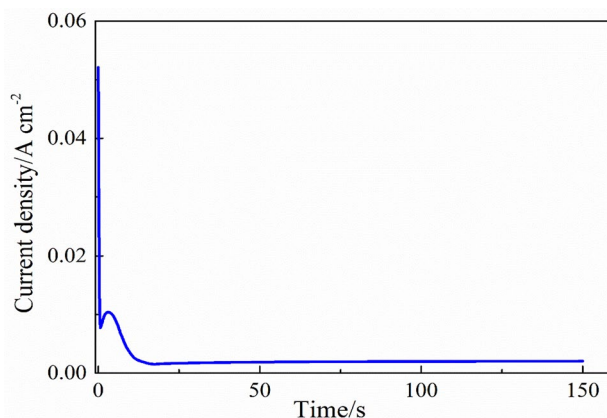

Fig. 3 Cyclic voltammetry of Pb in 100 mol m^{-3} NaOH solution, T = 25 °C, at a scan rate of 10 mV s^{-1}

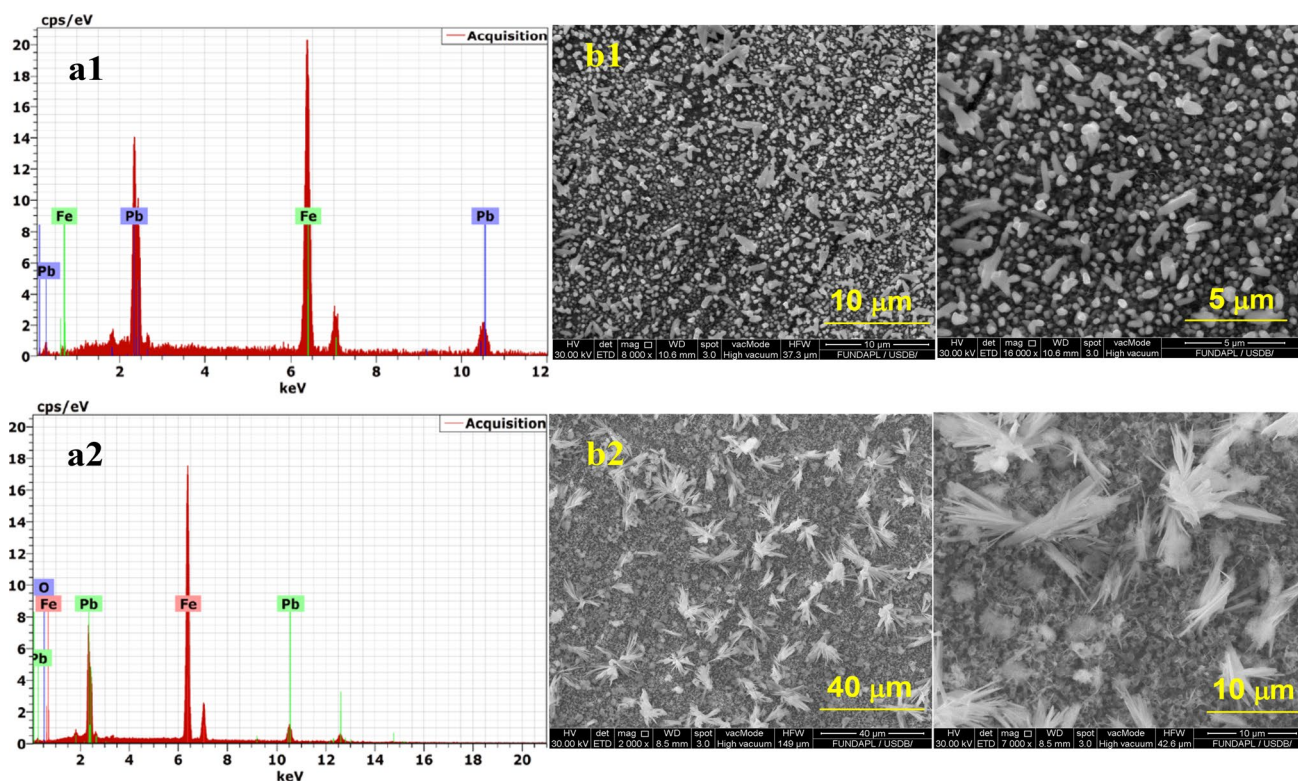**Fig. 4** Chronoamperometry of Pb in 100 mol m^{-3} NaOH solution, E = 0.7 V at 25 °C

Fig. 5 EDX spectrum of the quick-dried thin film (**a1**), the slowly air-dried thin film (**a2**), b) SEM images of the quick-dried thin film (**b1**), the slowly air-dried thin film (**b2**)
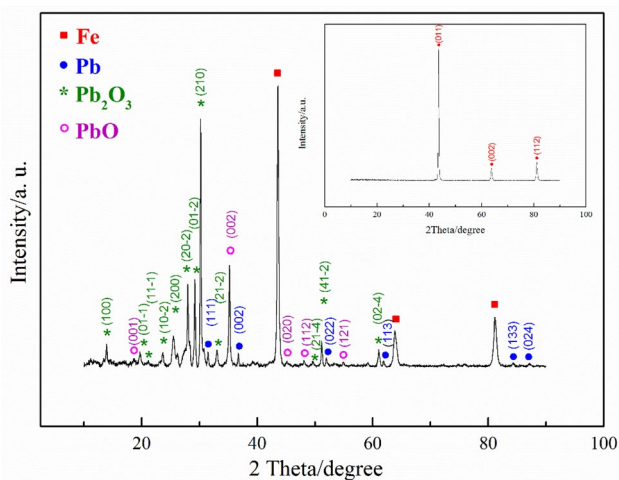

Fig. 6 The X-ray diffraction pattern of the thin film, under slowly air-drying electrode, (Inset the X-ray diffraction pattern of substrat Fe)

was performed. In order to identify the oxides formed in the air-dried sample, a DRX analysis was performed, the Fig. 6 shown the X-Ray pattern for the cathodic film.

The DRX spectrum of cathode film (Fig. 6) shows the presence of Fe peaks indexed according to JCPDS map No. 98-004-4863 and the presence of small lead metal

peaks No. 98-005-2253, and also lead oxides such as PbO litharge No. 98 001 5466 and Pb_2O_3 No. 98 002 3760. Iron presence in the modified electrode is due to substrate initially used. Our experiment has shown that the lead metal (wet) deposited on the working electrode of iron has been oxidized to PbO and Pb_2O_3 when removed from the cell, which is observed by the change of color after a short moment of its exposure to air (presence of oxygen). The presence of lead oxides in electrochemically deposited lead implies the formation of highly active rather than passive lead micro-particles, which react rapidly with oxygen [26]. This results confirmed that the formation of lead oxides has no relation to the generation of OH- formed by electroreduction of NO_3 and/or O_2 but rather a chemical reaction occurred when the electrodeposited lead metal film is removed from solution and dried in air converting it to lead oxide. It should, however, be noted that the presence of water should be important for this reaction to take place as it provides a medium of mass transport for the reaction [27].

The crystal form of the phase is verified by XRD (Fig. 7); the reflection conditions are in agreement with JCPDS map No. 98-002-0754 and all peaks are assigned to the alpha-PbO_2 crystal form, crystallizing in orthorhombic symmetry, which is in agreement with the literature. The lead dioxide
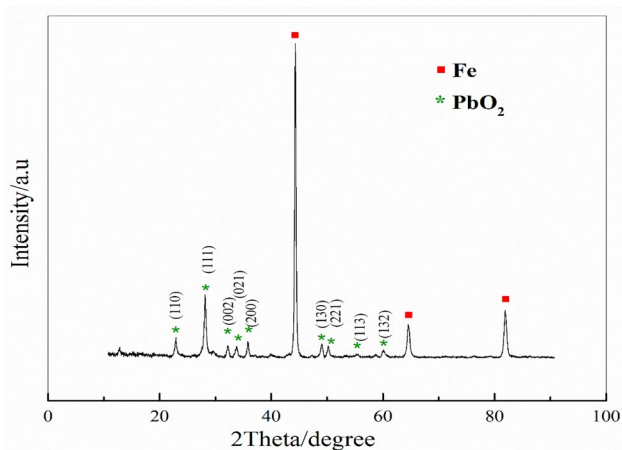
Fig. 7 The X-ray diffraction pattern of α-PbO$_2$

electrodeposited from acidic solution exists in β-PbO$_2$ form, but in basic solution α-PbO$_2$ is the major form.

3.3.1 Impedance spectroscopy

In the Nyquist plots (Fig. 8a), at high frequency, a semicircle is observed presenting the charge transfer resistance and at low frequency, a linear portion relates to the diffusion process. Figure 8b (insets) shows Randles equivalent electrical circuits with the Rs represent the resistance of the electrolyte, CPE the constant phase element for double-layer and Rct the charge transfer resistance at the electrode/electrolyte interface, and W the Warburg impedance related to the diffusion of ions in surface film. By fitting the Randles equivalent electrical circuits, the Rct values for Fe, Fe/Pb and Fe/Pb/

PbO$_2$ electrodes were found to be 490 ohms, 240 and 747 ohms, respectively [28, 29].

The PbO$_2$ modified electrode shows a large semicircle with a high charge transfer resistance Rct value, while the bare iron electrode and the lead film modified electrode show lower resistances, which indicate that the electrode has been effectively modified.

3.3.2 Accelerated lifetime

During the accelerated electrode lifetime test under conditions of high current density (1000 mA cm^{-2}), and high concentration (500 mol m^{-3}), the initial voltage of the Fe/Pb/α-PbO$_2$ electrode remains stable for 200 h, (Fig. 9). The voltage increased rapidly over the last 15 h. The lifetime of an electrode is given as the time when the practiced voltage increases by 5 V. Based on this definition, the Fe/Pb/α-PbO$_2$ electrode has a lifetime of 200 h [30].

3.4 Use of modified electrode in the electrodegradation of IC

Figure 10 shows the LSV of the Fe/Pb/α-PbO$_2$ modified electrode, and according to this polarization curve it is clearly shown that the Fe/Pb/α-PbO$_2$ modified electrode has a high oxygen release potential, starting from 1.5 V/SCE (Oxygen evolution overvoltage on PbO$_2$ is 0.51 V (NHE)) which leads to the production of adsorbed radicals (OH$^{\bullet}$) able to degrading organic pollutants due to their high oxidative power. In this context, the anodic oxidation of IC dye on Fe/Pb/α-PbO$_2$ has been studied [31].

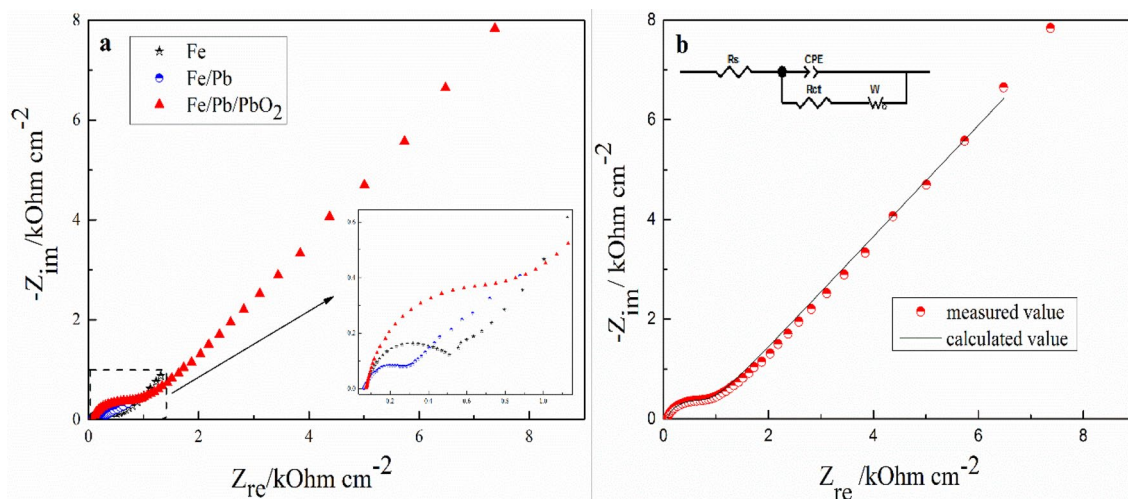During the oxidative degradation of pollutants by PbO$_2$ electrodes, they are mostly mineralized on the surface of

Fig. 8 Electrochimical impedance spectroscopy in 50 mol m^{-3} KNO$_3$ in a frequency range of 10^5—10^{-2} Hz nyquist diagram of Fe, Fe/Pb and Fe/Pb/PbO$_2$ electrodes (**a**), Fe/Pb/PbO$_2$ nyquist plot with the calculated value, insets: Randle's equivalent circuit for the system (**b**)
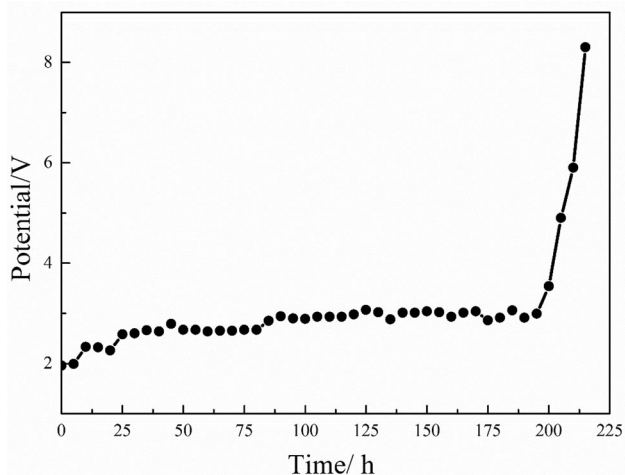
Fig. 9 Accelerated lifetime test in 500 mol m^{-3} KNO$_3$ with current density of 1000 mA cm^{-2} at 25 °C

Fig. 11 UV–Vis absorption spectra of 10^{-2} mol m^{-3} Indigo Carmin in 50 mol m^{-3} KNO$_3$ at different electrolysis time (0 – 60 min) and 2.4 V
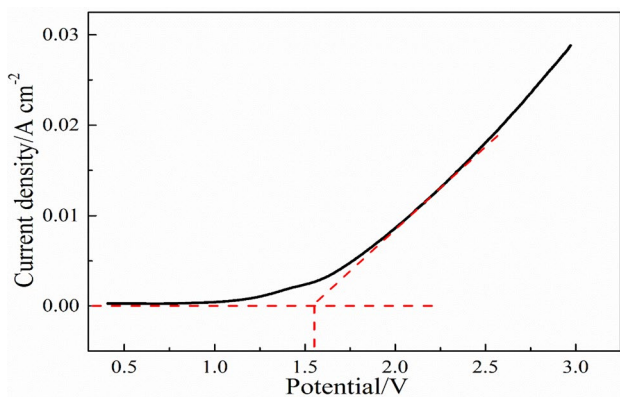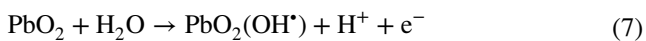

Fig. 10 Linear sweep voltammogram of PbO$_2$ electrode obtained in 50 mol m^{-3} KNO$_3$ with a scan rate of 25 mV s^{-1}, at 25 °C

Fig. 12 Degradation efficiency of 10^{-2} mol m^{-3} IC in 50 mol m^{-3} KNO$_3$, T = 25 °C

the electrode by the electro-generated (HO$^\bullet$) [32]. The initial reaction is the generation of adsorbed hydroxyl radical PbO$_2$(HO$^\bullet$) via the oxidation of water molecules Eq. (7).

$$PbO_2 + H_2O \rightarrow PbO_2(OH^\bullet) + H^+ + e^- \qquad (7)$$

In the next step, the electrochemically generated MOx (OH$^\bullet$) that is one of the strongest oxidant of organic matter (IC) Eq. (8) [33–35].

$$IC + PbO_2(OH^\bullet) \rightarrow intermediates \rightarrow\rightarrow\rightarrow CO_2 + H_2O \qquad (8)$$
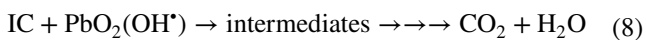
The UV–visible spectrum was used to follow the changes during the different period of electrochemical degradation of 10^{-2} mol m^{-3} IC at 2.4, 2.6, 2.8 V/SCE. The absorption peak of the IC before the treatment is at 610 nm as shown in the Fig. 11, During the degradation
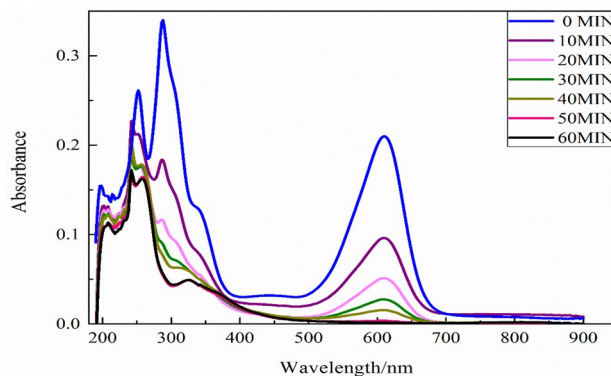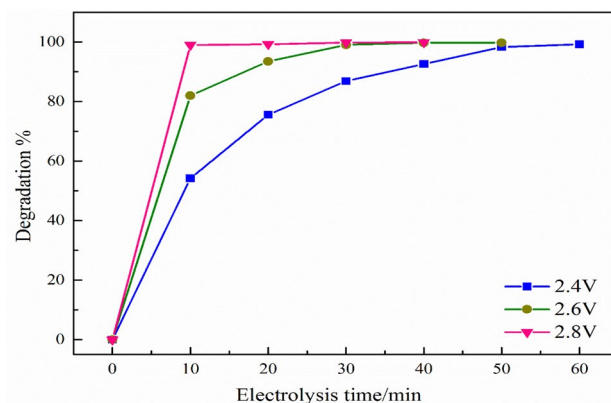
process, the absorption peaks decrease with the electrolysis time until they disappear, which shows the total degradation of IC dye.

The potential is a very important factor in the electrochemical degradation, as it controls the generation of hydroxyl radicals.

According to the Fig. 12, an increase in the cell voltage accelerates the oxidation reaction of IC, which is explained by the fact that at a higher potential the production of oxidative species increases. The degradation time is decreased from 60 min (E = 2.4 V/SCE) to 10 min by increasing the potential (2.8 V/SCE).

According to the Fig. 13, the degradation of IC dye follows pseudo-first-order reaction kinetics (Relation 9).

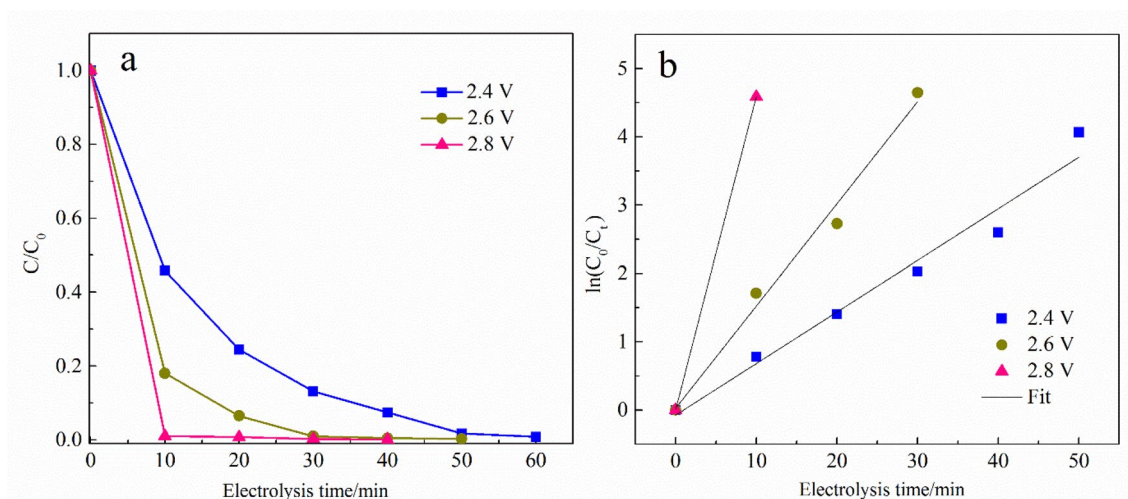$$\ln \frac{C_0}{C_t} = K_{app} t \qquad (9)$$

Fig. 13 Potential effect on the electrochemical oxidation of 10^{-2} mol m^{-3} IC in 50 mol m^{-3} KNO$_3$, T = 25 °C **(a)**, Pseudo first-order plot of degradation of 10^{-2} mol m^{-3} IC **(b)**

Table 1 Values of pseudo-first-order kinetics constants (K_{app}) and R^2 of dye degradation at different potentials

Potential V	Apparent constants min^{-1}	R^2
2.4	0.7 10^{-1}	0.96
2.6	1.4 10^{-1}	0.98
2.8	4.6 10^{-1}	1

By comparing fitted rate constant values of degradation (k), at different electrolyte potentials (Table 1), an increase in cell voltage is found to significantly accelerate the degradation of IC, and the k values increase from 0.07.548 cm^{-1} to 0.4585 cm^{-1} as the cell voltages increase from 2.4 V to 2,. V. At a lower potential, smaller number of oxidative species are produced, which is in agreement with the theory of electrochemistry.

To complete our study, we examined the influence of pH on the rate of IC degradation. Figure 14 shows the degradation rate of IC as a function of pH in the range of 3–9. The results indicate that a high electrocatalytic degradation efficiency is obtained in acidic solution, and the degradation efficiency at pH 3 is slightly lower than that at pH 5.7.

Figure 14 shows that the degradation under different pH follows the pseudo-first order reaction kinetics. The values of k and R^2 listed in Table 2 also prove that the degradation under acidic condition is better than that under neutral or basic condition and considering that most wastewater is a neutral solution, pH 5.7 of the initial solution (without prior adjustment) is chosen as the optimal pH for electrocatalytic degradation of IC (Fig. 15).

According to the above results, the total organic carbon analysis was performed for the best degradation solution
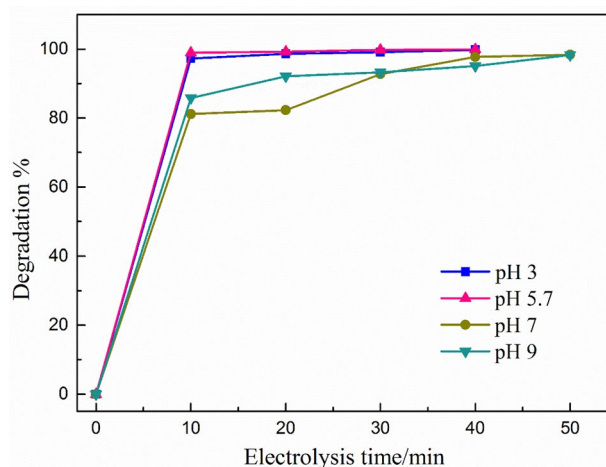

Fig. 14 Effect of pH on the degradation efficiency of 10^{-2} mol m^{-3} IC in 50 mol m^{-3} KNO$_3$, T = 25 °C

Table 2 Values of pseudo-first-order kinetics constants (K_{app}) and R^2 of dye degradation at different pH

pH	Apparent constants min^{-1}	R^2
3	3.6 10^{-1}	1
5.7	4.6 10^{-1}	1
7	1.03 10^{-1}	0.94
9	0.9 10^{-1}	0.91

at pH = 5.7 and E = 2.8 V before and after degradation. The TOC results showed the total absence of organic carbon after 10 min of degradation, which shows a total mineralization, compared to other works this novel electrode gives very good IC degradation results. A comparative
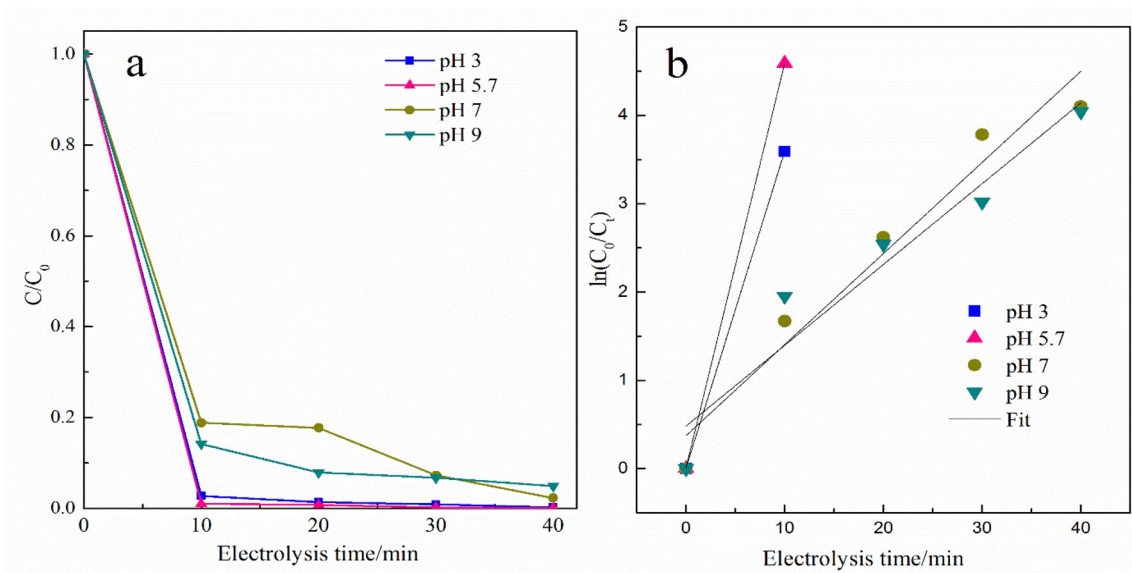
Fig. 15 Effect of pH on the electrochemical oxidation of 10^{-2} mol m^{-3} IC in 50 mol m^{-3} KNO$_3$, T = 25 °C **(a)**, Pseudo first-order plot of degradation of 10^{-2} mol m^{-3} IC **(b)**

study with other IC degradation works at different processes is presented in Table 3.

In this work, HO$^{\bullet}$ are considered as the active radicals during IC decomposition, Fig. 16 shows the trapping experiment carried out in the presence of 10^3 mol m^{-3} and $2 \cdot 10^3$ mol m^{-3} HO$^{\bullet}$ scavenger isopropanol. The degradation efficiency of IC decreases from 99 to 50% and to 34% when 10^3 mol m^{-3} and $2 \cdot 10^3$ mol m^{-3} isopropanol respectively introduced into the electrocatalytic degradation system, indicating that HO$^{\bullet}$ is determined to be the active species in electrocatalytic degradation process of IC.

4 Conclusion

In our work we have shown that the electrodeposited (wet) lead metal oxidizes to lead oxide by drying it slowly in the air (presence of oxygen), as this oxidation can be stopped by drying it quickly after removing it from the solution.

It can also be concluded that a lead oxides film can be formed by metallic reduction of Pb(II) in a lead nitrate solution, and this one has no relation with the formation of OH- in solution, which implies the formation of lead hydroxide, this means that the metallic lead was initially deposited and then oxidized in the presence of oxygen in air. This was confirmed by EDX analysis which showed the presence of a metallic lead film on the rapidly dried electrode, however the presence of lead and oxygen on the slowly air-dried sample,

Table 3 Comparative study of IC degradation

| Procedure	Color removal %	Time (min)	References
Low voltage pulse electrolysis RuO2-IrO2-SnO2	50	180	[36]
Photocatalysis ZnO–Bi$_2$O$_3$–2C$_3$N$_4$/H$_2$O$_2$/Vis	93	18	[37]
ZnO-Fe$_3$O$_4$/ Kal/solar irradiation	100	70	[38]
AgIO$_4$/ZnO/Hg lamp 365 nm	95	160	[39]
ZnFe$_2$O$_4$/ZnO/UV light	99	90	[40]
Photo-Fenton/ H$_2$O$_2$/UV-C	70	60	[41]
Electrochemical-doped Sb$_2$O$_3$ Ti/IrO$_2$-SnO$_2$	75	420	[42]
Ozonolysis/UV	97.3	10	[43]
Electrocoagulation	80	240	[44]
Electrochemical Fe/Pb/PbO$_2$	100	10	This work
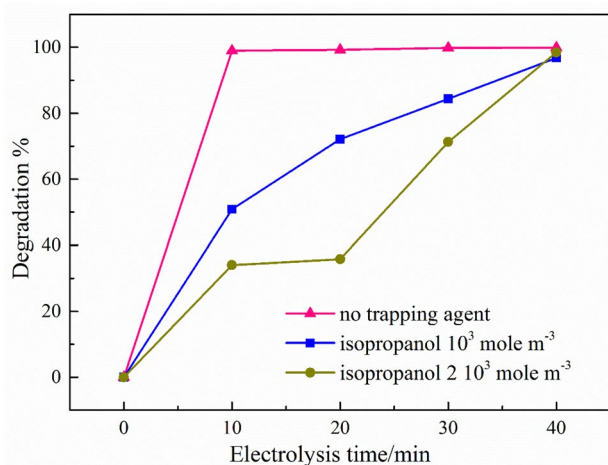
Fig. 16 Degradation curve of 10^{-2} mol m^{-3} IC in 50 mol m^{-3} KNO$_3$ in the presence of trapping reagent T = 25 °C

the oxides formed were identified by X-ray diffraction which showed the formation of PbO and Pb$_2$O$_3$.

Lead dioxide was formed by anodization of lead metal film in basic 0.1 M NaOH solution, the result of XRD showed the formation of α-PbO$_2$ crystal structure. Due to its highest overpotential for oxygen evolution (0.51 V (ENH)) and its excellent electrocatalytic activity, the electrode modified by α-PbO$_2$ film has been tested for the electrochemical degradation of Indigo Carmine. The formation of OH$^\bullet$ by oxidation of water on α-PbO$_2$ plays a role of intermediary able to degrading the totality of dye due to their high oxidizing power, and their reactivity.

The electrochemical oxidation of Indigo Carmine using α-PbO$_2$ gave an excellent result translated by a total degradation due to the formation of hydroxyl radicals from the water oxidation, the latter followed a pseudo-first order kinetics.

The applied potential had a significant effect on the electrochemical degradation of Indigo Carmine at the α-PbO$_2$ electrode, such that the IC removal rate increased with the increase in applied potential. After 10 min of electrolysis at constant potential, the IC removal rates reached 54%, 81%, and 99% at potentials of 2.4, 2.6 and 2.8 V/SCE, respectively, as well as the degradation was better in acidic solutions.

Declarations

Conflict of interest The authors declare that they have no conflict of interest.

References

1. Zhang Q, Yao C, Hong J-M, Chang C-T (2019) Preparation of Pt/TiO 2 /graphene/polyethylene sheets via a facile molding process for Azo dye electrodegradation. J Nanosci Nanotechnol 20:3287–3294
2. Wang M-X, Zhang Q-L, Yao S-J (2015) A novel biosorbent formed of marine-derived Penicillium janthinellum mycelial pellets for removing dyes from dye-containing wastewater. Chem Eng J 259:837–844
3. Kornaros M, Lyberatos G (2006) Biological treatment of wastewaters from a dye manufacturing company using a trickling filter. J Hazard Mater 136:95–102
4. Khayet M, Zahrim AY, Hilal N (2011) Modelling and optimization of coagulation of highly concentrated industrial grade leather dye by response surface methodology. Chem Eng J 167:77–83
5. Jiang W, Zhang W, Li B, Duan J, Lv Y, Liu W, Ying W (2011) Combined fenton oxidation and biological activated carbon process for recycling of coking plant effluent. J Hazard Mater 189:308–314
6. Zahrim AY, Hilal N (2013) Treatment of highly concentrated dye solution by coagulation/flocculation–sand filtration and nanofiltration. Water Resour Ind 3:23–34
7. Li P, Zhao G, Zhao K, Gao J, Wu T (2012) An efficient and energy saving approach to photocatalytic degradation of opaque high-chroma methylene blue wastewater by electrocatalytic pre-oxidation. Dye Pigment 92:923–928
8. Saaidia S, Delimi R, Benredjem Z, Mehellou A, Djemel A, Barbari K (2017) Use of a PbO2 electrode of a lead-acid battery for the electrochemical degradation of methylene blue. Sep Sci Technol 52:1602–1614
9. Heck KN, Garcia-Segura S, Westerhoff P, Wong MS (2019) Catalytic converters for water treatment. Acc Chem Res 52:906–915
10. Li X, Pletcher D, Walsh FC (2011) Electrodeposited lead dioxide coatings. Chem Soc Rev 40:3879–3894
11. Zhang Y, He P, Jia L, Li C, Liu H, Wang S, Zhou S, Dong F (2019) Ti/PbO2-Sm2O3 composite based electrode for highly efficient electrocatalytic degradation of alizarin yellow R. J Colloid Interface Sci 533:750–761
12. Zhu W, Zhang R, Qu F, Asiri AM, Sun X (2017) Design and application of foams for electrocatalysis. ChemCatChem 9:1721–1743
13. Yao Y, Huang C, Dong H, Wei F, Chen X (2019) Influence of manganese ions on the electrodeposition process of lead dioxide in lead nitrate solution. Russ J Electrochem 55:364–369
14. Burazer S, Sopčić S, Mandić Z (2016) Anodic deposition of lead dioxide at Nafion® covered gold electrode. J Solid State Electrochem 20:3053–3059
15. Hwang BJ, Santhanam R, Chang YW (2002) Mechanism of electrodeposition of PbO2 at a Pt sheet/rotating disk electrode. Electroanal Int J Devoted Fundam Pract Asp Electroanal 14:363–367
16. Dargahi A, Ansari A, Nematollahi D, Asgari G, Shokoohi R, Samarghandi MR (2019) Parameter optimization and degradation mechanism for electrocatalytic degradation of 2,4-diclorophenoxyacetic acid (2,4-D) herbicide by lead dioxide electrodes. RSC Adv 9:5064–5075
17. Wu X, Xu H, Lu L, Zhao H, Fu J, Shen Y, Xu P, Dong Y (2014) PbO2-modified graphite felt as the positive electrode for an all-vanadium redox flow battery. J Power Sources 250:274–278

18. Pereira JF, Figueiredo RS, Ponce-de-León C, Bertazzoli R (2016) Platinum-free lead dioxide electrode for electrooxidation of organic compounds. J solid state Electrochem 20:1167–1173

19. Smaili F, Benchettara A (2019) Electrocatalytic efficiency of PbO 2 in water decontamination. Russ J Electrochem 55:925–932

20. Velayutham D, Noel M (1991) The influence of electrolyte media on the deposition-dissolution behaviour of lead dioxide on glassy carbon electrode. Electrochim Acta 36:2031–2035

21. Velichenko AB, Girenko DV, Danilov FI (1996) Mechanism of lead dioxide electrodeposition. J Electroanal Chem 405:127–132

22. Velichenko AB, Amadelli R, Gruzdeva EV, Luk'yanenko TV, Danilov FI (2009) Electrodeposition of lead dioxide from methanesulfonate solutions. J Power Sources 191:103–110

23. Knysh V, Luk'yanenko T, Shmychkova O, Amadelli R, Velichenko A (2017) Electrodeposition of composite PbO 2–TiO 2 materials from colloidal methanesulfonate electrolytes. J Solid State Electrochem 21:537–544

24. Labiadh L, Barbucci A, Carpanese MP, Gadri A, Ammar S, Panizza M (2017) Direct and indirect electrochemical oxidation of Indigo Carmine using PbO2 and TiRuSnO2. J Solid State Electrochem 21:2167–2175

25. Zhou D, Gao L (2007) Effect of electrochemical preparation methods on structure and properties of PbO2 anodic layer. Electrochim Acta 53:2060–2064

26. Bhatt AI, Bond AM, Zhang J (2007) Electrodeposition of lead on glassy carbon and mercury film electrodes from a distillable room temperature ionic liquid, DIMCARB. J Solid State Electrochem 11:1593–1603

27. Sawatani S, Ogawa S, Yoshida T, Minoura H (2005) Formation of highly crystallized β-PbO thin films by cathodic electrode position of Pb and its rapid oxidation in air. Adv Funct Mater 15:297–301

28. Saidin MI, Isa IM, Ahmad M, Hashim N, Ab Ghani S (2017) Analysis of trace nickel by square wave stripping voltammetry using chloropalladium(II) complex-modified MWCNTs paste electrode. Sensors Actuators, B Chem 240:848–856

29. Nodehi M, Baghayeri M, Veisi H (2021) Preparation of GO/Fe3O4@PMDA/AuNPs nanocomposite for simultaneous determination of As3+ and Cu2+ by stripping voltammetry. Talanta 230:122288

30. Jin H, Zhang X, Yu Y, Chen X (2022) High-performance Ti/IrO2-RhOx-TiO2/α-PbO2/β-PbO2 electrodes for scale inhibitors degradation. Chem Eng J 435:135167

31. Xu M, Wang Z, Wang F, Hong P, Wang C, Ouyang X, Zhu C, Wei Y, Hun Y, Fang W (2016) Fabrication of cerium doped Ti/nanoTiO2/PbO2 electrode with improved electrocatalytic activity and its application in organic degradation. Electrochim Acta 201:240–250

32. Mahmoudpoor Moteshaker P, Saadi S, Rokni SE (2020) Electrochemical removal of diazinon insecticide in aqueous solution by Pb/β-PbO2 anode. Effect of parameters and optimization using response surface methodology. Water Environ Res 92:975–986

33. Brillas E, Martínez-Huitle CA (2015) Decontamination of wastewaters containing synthetic organic dyes by electrochemical methods. An updated review. Appl Catal B Environ 166:603–643

34. Dai Q, Zhou J, Weng M, Luo X, Feng D, Chen J (2016) Electrochemical oxidation metronidazole with Co modified PbO2 electrode: Degradation and mechanism. Sep Purif Technol 166:109–116

35. Martínez-Huitle CA, Rodrigo MA, Sires I, Scialdone O (2015) Single and coupled electrochemical processes and reactors for the abatement of organic water pollutants: a critical review. Chem Rev 115:13362–13407

36. Zhan W, Du Y, Lan J, Lei R, Li R, Du D, Zhang TC (2022) Electrochemical degradation of indigo carmine by low voltage pulse electrolysis. J Mol Liq 348:118006

37. Huy BT, Paeng DS, Thi Bich Thao C, Kim Phuong NT, Lee YI (2020) ZnO-Bi2O3/graphitic carbon nitride photocatalytic system with H2O2-assisted enhanced degradation of Indigo carmine under visible light. Arab J Chem 13:3790–3800

38. Hadjltaief HB, Bairq ZAS, Shi C, Benzina M (2021) Evaluation of sono-assisted solar/Fenton process for indigo carmine degradation over magnetic ZnO-Fe3O4 supported Tunisian kaolinite clay. Surfaces and Interfaces 26:101395

39. Abdel-Aziz R, Ahmed MA, Abdel-Messih MF (2020) A novel UV and visible light driven photocatalyst AgIO4/ZnO nanoparticles with highly enhanced photocatalytic performance for removal of rhodamine B and indigo carmine dyes. J Photochem Photobiol A Chem 389:112245

40. Güy N, Özacar M (2018) Visible light-induced degradation of indigo carmine over ZnFe2O4/Tannin/ZnO: role of tannin as a modifier and its degradation mechanism. Int J Hydrogen Energy 43:8779–8793

41. Ramos RO, Albuquerque MVC, Lopes WS, Sousa JT, Leite VD (2020) Degradation of indigo carmine by photo-Fenton, Fenton, H2O2/UV-C and direct UV-C: Comparison of pathways, products and kinetics. J Water Process Eng 37:101535

42. Palma-Goyes RE, Silva-Agredo J, Vazquez-Arenas J, Romero-Ibarra I, Torres-Palma RA (2018) The effect of different operational parameters on the electrooxidation of indigo carmine on Ti/IrO2-SnO2-Sb2O3. J Environ Chem Eng 6:3010–3017

43. Crema APS, Piazza Borges LD, Micke GA, Debacher NA (2020) Degradation of indigo carmine in water induced by non-thermal plasma, ozone and hydrogen peroxide: a comparative study and by-product identification. Chemosphere 244:125502

44. Donneys-Victoria D, Bermúdez-Rubio D, Torralba-Ramírez B, Marriaga-Cabrales N, Machuca-Martínez F (2019) Removal of indigo carmine dye by electrocoagulation using magnesium anodes with polarity change. Environ Sci Pollut Res 26:7164–7176